AIAA JOURNAL
Vol. 47, No. 10, October 2009

Time-Domain Impedance Boundary Conditions for Simulations of Outdoor Sound Propagation

Benjamin Cotté,* Philippe Blanc-Benon,† and Christophe Bogey‡
École Centrale de Lyon, 69134 Écully Cedex, France
and
Franck Poisson§
Société Nationale des Chemins de Fer, 75379 Paris Cedex 08, France

DOI: 10.2514/1.41252

Finite difference time-domain methods are well suited to study sound propagation in the context of transportation noise. In this paper, time-domain boundary conditions are considered for impedance models classically used for outdoor grounds. These impedance models have usually been obtained in the frequency domain and cannot be translated directly into the time domain. The derivation of the time-domain boundary condition is based on the approximation of the impedance as a sum of well-chosen template functions. Because of the forms of the template functions, the recursive convolution technique can be applied; this is a fast and computationally efficient method to calculate a discrete convolution. The impedance boundary conditions are validated using a linearized Euler equations solver in one- and three-dimensional geometries; comparisons with analytical solutions in the time and frequency domains are presented. The methods used to identify the coefficients of the template functions are shown to be of great importance. Among the three methods described, the optimization method in the frequency domain can be recommended, because it can be applied to many impedance models and allows the values of the coefficients to be constrained, which is needed to obtain accurate numerical results.

Nomenclature

B	=	Gaussian half-width, m
c_0	=	speed of sound, m/s
d_L	=	porous layer thickness, m
f	=	frequency, Hz
Im[]	=	imaginary part
j	=	imaginary unit
k	=	complex wave number, m^{-1}
p	=	pressure, Pa
q	=	tortuosity
Re[]	=	real part
S	=	number of first-order systems in the impedance approximation
s_f	=	coefficient of the selective filter
T	=	number of second-order systems in the impedance approximation
t	=	time, s
v	=	velocity component normal to impedance surface, m/s
Z	=	complex impedance, $kg/m^2/s$
γ	=	ratio of specific heats
ΔL	=	sound pressure level relative to the free field, dB
Δt	=	time step, s
Δx	=	spatial mesh size, m
ρ_0	=	air density, kg/m^3
σ_0, σ_e	=	flow resistivity, $Pa \cdot s/m^2$
Ω	=	porosity
ω	=	angular frequency, rad/s

Presented as Paper 3021 at the 14th AIAA/CEAS Aeroacoustics Conference, Vancouver, BC, Canada, 5–7 May 2008; received 26 September 2008; revision received 26 February 2009; accepted for publication 26 February 2009.

*Ph.D. Student, Centre National de la Recherche Scientifique, Laboratoire de Mécanique des Fluides et d'Acoustique, Unité Mixte de Recherche 5509; benjamin.cotte@ec-lyon.fr. Member AIAA.

†Senior Research Scientist, Centre National de la Recherche Scientifique, Laboratoire de Mécanique des Fluides et d'Acoustique, Unité Mixte de Recherche 5509; philippe.blanc-benon@ec-lyon.fr. Member AIAA.

‡Research Scientist, Centre National de la Recherche Scientifique, Laboratoire de Mécanique des Fluides et d'Acoustique, Unité Mixte de Recherche 5509; christophe.bogey@ec-lyon.fr. Member AIAA.

§Research Engineer, Direction de l'Innovation et de la Recherche; franck.poisson@sncf.fr.

I. Introduction

TIME-DOMAIN numerical solutions of the linearized Euler equations (LEE) are well suited to study broadband noise propagation outdoors, because they can take into account the interactions of the acoustic waves with local wind and temperature fluctuations in the atmospheric boundary layer. The motion of the acoustic sources can also be considered with this type of simulation, which can be useful in the context of transportation noise. Finite difference time-domain methods are thus becoming increasingly popular in the outdoor sound propagation community [1,2]. However, obtaining a time-domain boundary condition (TDBC) for a ground of finite impedance is not straightforward. Indeed, impedance models classically used for outdoor grounds have been obtained in the frequency domain [3–6], and most of them cannot be translated directly into the time domain. To translate a frequency-domain impedance boundary condition to the time domain, the definition of impedance has to be extended to the whole complex frequency plane [7]. Using the $\exp(-j\omega t)$ convention, this leads to these necessary conditions for an impedance model to be physically possible [7] (where Re[] and Im[] correspond to the real and imaginary parts of a complex number, and $*$ means *complex conjugate of*):

1) For the causality condition, $Z(\omega)$ is analytic and nonzero in $\mathrm{Im}(\omega) > 0$.

2) For the reality condition, $Z^*(\omega) = Z(-\omega)$.

3) For the passivity condition, $\mathrm{Re}[Z(\omega)] \geq 0$.

The causality condition implies that the real and imaginary parts of the impedance are related by a Hilbert transform [8–10].

Several authors have proposed techniques to model the impedance of lining materials in the time domain [11–14]. These techniques have been applied with some success in duct acoustics configurations, but it is not clear how they would perform with ground impedance models. Also, it must be noted that these studies were

aiming at developing a TDBC in the presence of a mean flow. This is not an issue outdoors because the wind speed in the surface layer of the atmospheric boundary layer is quite low; typically, the corresponding Mach number is lower than 0.05. In addition, in the outdoor sound propagation community, several studies have aimed at modeling sound propagation over an impedance ground in the time domain using two different approaches. Some authors chose to add a porous layer to the computation domain and calculated sound propagation in the porous medium explicitly [1], whereas others developed TDBC from a classical ground impedance model, such as the phenomenological Zwikker and Kosten (ZK) model [2,15].

In this paper we follow the latter approach because it avoids extra calculations in the porous medium. First, following Reymen et al. [14], we will show that the impedance can be approximated by a set of well-chosen template functions for which the coefficients can be selected so that the causality, reality, and passivity conditions are met. A general TDBC is then obtained using the recursive convolution method originally developed in the context of electromagnetic propagation [16]; this is a fast and computationally efficient method to calculate a discrete convolution. It will be shown that the TDBC obtained by Ostashev et al. [15], starting from the unit impulse response of the impedance in the time domain, is quite similar to this general TDBC. Second, different identification methods will be proposed to find the coefficients of the template functions. The identification process can be performed in the frequency domain, as done by Fung and Ju [13] or Reymen et al. [14], or in the time domain, as done by Ostashev et al. [15]. It will appear that additional constraints on the value of the coefficients are required to ensure stability and good accuracy. Thus, the coefficient identification must be performed with great care to obtain both a good approximation of the impedance over the frequency band of interest and coefficient values that are suitable for numerical simulations.

In Sec. II of this paper, several ground impedance models that are commonly used in the frequency domain are reviewed. These are simple models, with no more than two adjustable parameters. Then, in Sec. III, the general TDBC is derived and compared with other TDBC found in the literature. Different methods of coefficient identification are also presented. In Sec. IV, the TDBC is validated in a LEE solver. One- and three-dimensional test cases are considered in Secs. IV.B and IV.C, respectively. Finally, a calculation is performed in Sec. IV.D for a configuration that is more realistic in the context of outdoor sound propagation.

II. Ground Impedance Models in the Frequency Domain

One of the most popular model used to calculate the impedance of outdoor grounds is the empirical Delany–Bazley (DB) model [4]. For a semi-infinite ground layer, the characteristic impedance has the following form:

$$Z/\rho_0 c_0 = 1 + a(f/\sigma_e)^b + jc(f/\sigma_e)^d \tag{1}$$

where ρ_0 is the air density; c_0 is the sound speed in the air; f is the frequency; σ_e is an effective flow resistivity; and a, b, c, and d are empirical coefficients. This is a simple one-parameter model that has been extensively used to model the impedance of grassland [17–19], although originally developed for fibrous absorbing materials.

A two-parameter impedance model can be built on the basis of Eq. (1), considering a rigidly backed layer of thickness d_L. The characteristic impedance is then written [18]

$$Z_L = jZ/\tan(kd_L) \tag{2}$$

where k is the complex wave number in the porous layer, which has the following form in the DB model:

$$k = \frac{\omega}{c_0}[1 + p(f/\sigma_e)^q + jr(f/\sigma_e)^s] \tag{3}$$

where p, q, r, and s are empirical coefficients. This ground impedance model has two adjustable parameters, σ_e and d_L.

For the classical DB model, the empirical coefficients in Eqs. (1) and (3) in SI units are

$$a_{\mathrm{DB}} = 0.0511, \qquad c_{\mathrm{DB}} = 0.0768$$
$$b_{\mathrm{DB}} = -0.75, \qquad d_{\mathrm{DB}} = -0.73 \tag{4}$$

$$p_{\mathrm{DB}} = 0.0858, \qquad r_{\mathrm{DB}} = 0.175$$
$$q_{\mathrm{DB}} = -0.70, \qquad s_{\mathrm{DB}} = -0.59 \tag{5}$$

Miki [9] showed that this choice of coefficients breaks the causality condition for an impedance model to be physically possible. He proposed new coefficients in Eqs. (1) and (3) to obtain an impedance model verifying the causality, reality, and passivity conditions:

$$a_M = 0.0699, \quad c_M = 0.107, \quad b_M = -0.632 \quad d_M = b_M \tag{6}$$

$$p_M = 0.109, \quad r_M = 0.160, \quad q_M = -0.618 \quad s_M = q_M \tag{7}$$

Figure 1 compares the normalized impedance of a rigidly backed layer of thickness, 0.01 m, and effective flow resistivity, 100 kPa · s · m^{-2}, using the DB or Miki model. Below 300 Hz, it appears that the real part of the impedance is negative using the DB model; thus, the ground is not passive anymore. Using the Miki model, the real part of the impedance remains positive on the frequency band 50–5000 Hz.

Recently, Wilson et al. [2] and Ostashev et al. [15] developed TDBC based on the phenomenological ZK model [3]. The characteristic impedance for a semi-infinite ground layer has the following form:

$$Z = Z_\infty \sqrt{\frac{1 - j\omega\tau}{-j\omega\tau}} \tag{8}$$

where Z_∞ and τ are the parameters of the model. With classical parameter values of the ZK model, the impedance is not correctly predicted at high frequencies or low flow resistivity. Thus, Wilson et al. [2] suggested the following parameter values:

$$Z_\infty = \frac{\rho_0 c_0}{\Omega}, \qquad \tau = \frac{\rho_0 q^2 \gamma}{\sigma_0 \Omega} \tag{9}$$

where Ω is the porosity of the ground, q is the tortuosity, σ_0 is the flow resistivity in the limit of low frequency, and γ is the ratio of specific heats for air. With this choice of parameters, the model, called modified ZK model, compares well to more sophisticated models (microstructural and relaxation models), and has a broader range of applications than the DB model, especially at low frequencies and for materials with high flow resistivity such as soil and asphalt [2].

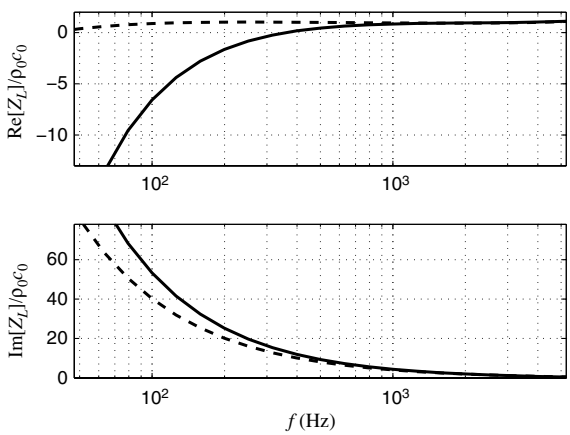

Fig. 1 Real and imaginary parts of the normalized impedance of a rigidly backed layer of thickness 0.01 m and effective flow resistivity 100 kPa · s · m^{-2}: DB model (solid line) and Miki model (dashed line).

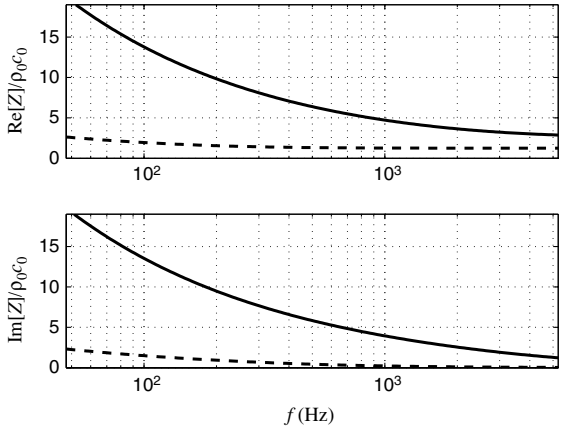

Fig. 2 Real and imaginary parts of the normalized impedance using the modified ZK model for a semi-infinite layer: soft soil ($\sigma_0 = 200\ \mathrm{kPa \cdot s \cdot m^{-2}}$, $\Omega = 0.5$, and $q = 1.3$) (solid line) and snow ($\sigma_0 = 5\ \mathrm{kPa \cdot s \cdot m^{-2}}$, $\Omega = 0.8$, and $q = 1$) (dashed line).

However, the modified ZK model should be avoided to calculate the impedance of grounds with an inhomogeneous structure, such as the rigidly backed layer of Eq. (2), because it yields predictions of the complex wave number that are significantly different from more sophisticated model predictions (see attenuation prediction comparisons done by Wilson et al. in [20]. Figure 2 shows the frequency dependence of the normalized impedance using the modified ZK model with porous material parameters typical of soft soil and snow.

III. Derivation of Time-Domain Impedance Boundary Conditions

Let $p(t)$ be the acoustic pressure and $v(t)$ the component of particle velocity normal to the interface between the ground and the air, with $P(\omega)$ and $V(\omega)$ their respective Fourier transform. The frequency-domain boundary condition

$$P(\omega) = Z(\omega)V(\omega) \tag{10}$$

can be translated into the time domain yielding the following TDBC:

$$p(t) = \int_{-\infty}^{+\infty} v(t-t')z(t')\,\mathrm{d}t' \tag{11}$$

where $z(t)$ is the inverse Fourier transform of the impedance $Z(\omega)$. To avoid the calculation of the convolution in Eq. (11), which is not efficient from a numerical point of view, it has been suggested to use the recursive convolution (RC) method introduced by Luebbers and Hunsberger [16] in the context of electromagnetic propagation through dispersive media. The RC method can be applied through the use of special functions corresponding to Debye and Lorentz dispersive media in electromagnetics [16]. To introduce these functions, some kind of approximation needs to be done. In Sec. III.A, the impedance is approximated in the frequency domain, following a method proposed by Fung and Ju [13] and also used by Reymen et al. [14]. The frequency-domain approximation can be applied to any impedance model. In Sec. III.B, the approximation is performed in the time domain, following a technique that Ostashev et al. [15] applied on the modified ZK impedance model. The response function $z(t)$ must be known analytically to use the time-domain approximation. It will be shown that this function can be calculated for the Miki model of a semi-infinite ground layer. Finally, in Sec. III.C, three methods that can be used to identify the coefficients appearing in the TDBC are presented.

A. Frequency-Domain Approximation

Following Reymen et al. [14], the impedance is written as the sum of S first-order systems (real poles) and T second-order systems (complex conjugated poles):

$$Z(\omega) = \sum_{k=1}^{S} Z_k(\omega) + \sum_{l=1}^{T} Z_l(\omega) \tag{12}$$

The impedance $Z_k(\omega)$ and the corresponding unit impulse response $z_k(t)$ for a real pole $\lambda_k > 0$ are

$$Z_k(\omega) = \frac{A_k}{\lambda_k - j\omega} \tag{13}$$

$$z_k(t) = A_k e^{-\lambda_k t} H(t), \qquad \lambda_k \geq 0 \tag{14}$$

where $H(t)$ is the Heaviside function, which is zero for $t < 0$ and one otherwise. The impedance $Z_l(\omega)$ and the corresponding unit impulse response $z_l(t)$ for a pair of complex conjugated poles λ_l and λ_l^*, written $\alpha_l \pm j\beta_l$, are

$$Z_l(\omega) = \frac{A_l}{\lambda_l - j\omega} + \frac{B_l}{\lambda_l^* - j\omega} = \frac{D_l - jC_l}{(\alpha_l - j\omega)^2 + \beta_l^2} \tag{15}$$

$$z_l(t) = e^{-\alpha_l t} H(t)\left[C_l \cos(\beta_l t) + \frac{D_l - \alpha_l C_l}{\beta_l}\sin(\beta_l t)\right], \qquad \alpha_l \geq 0 \tag{16}$$

From Eq. (15),

$$C_l = A_l + B_l \tag{17}$$

$$D_l = \alpha_l(A_l + B_l) + j\beta_l(B_l - A_l) \tag{18}$$

Thus, we must have $B_l = A_l^*$ for C_l and D_l to be real, which is a necessary condition for the impedance model given by Eqs. (12–16) to be real. This impedance model is also causal if the conditions $\lambda_k \geq 0$ and $\alpha_l \geq 0$ are met and it is passive for a good choice of the coefficients.

The impedance model given by Eqs. (12–16) was originally proposed by Fung and Ju [13], who used similar template functions to approximate the reflection coefficient. Their model relates the incoming and outgoing velocities, whereas the model proposed here relates the pressure and the normal velocity. Note also that the mass-spring-damper model used by Tam and Auriault [11], Özyörük and Long [12], and Fung and Ju [13] can be written as a second-order system of the form of Eq. (15) [14]. This is a three-parameter model that is able to match any given impedance at a single frequency.

Let us now consider the variables $p^{(n)} = p(n\Delta t)$ and $v^{(n)} = v(n\Delta t)$ in their discretized form, with Δt as the time step. Because of the special form of the template functions $z_k(t)$ and $z_l(t)$, the RC method can be used and the following TDBC is obtained [14]:

$$p^{(n)} = \sum_{k=1}^{S} A_k \phi_k^{(n)} + \sum_{l=1}^{T} C_l \,\mathrm{Re}[\psi_l^{(n)}] + \frac{D_l - \alpha_l C_l}{\beta_l}\,\mathrm{Im}[\psi_l^{(n)}] \tag{19}$$

where ϕ_k and ψ_l are accumulators given by

$$\phi_k^{(n)} = v^{(n)}\frac{1 - e^{-\lambda_k \Delta t}}{\lambda_k} + \phi_k^{(n-1)} e^{-\lambda_k \Delta t} \tag{20}$$

$$\psi_l^{(n)} = v^{(n)}\frac{1 - e^{-(\alpha_l - j\beta_l)\Delta t}}{\alpha_l - j\beta_l} + \psi_l^{(n-1)} e^{-(\alpha_l - j\beta_l)\Delta t} \tag{21}$$

Equations (20) and (21) are obtained assuming the velocity is constant over a time step Δt, which is referred to as the piecewise constant RC method, in contrast with the piecewise linear RC method proposed by Kelley and Luebbers [21]. Equations (19–21) show that the RC method is a very computationally efficient algorithm. If only real poles are considered, S real-valued accumulators ϕ_k are introduced. T complex-valued accumulators ψ_l are also introduced if complex conjugated poles are considered, and only two storage locations per accumulator are needed. Finally, we will see in

Sec. IV.A that this TDBC can be included in the optimized Runge–Kutta scheme used for time integration in the LEE solver.

B. Time-Domain Approximation

Ostashev et al. [15] proposed a method to derive a TDBC for the modified ZK model. This method is based on an approximation in the time domain. In a first step, the impedance given by Eq. (8) is converted to the time domain by inverse Fourier transform, and in a second step, the slow decaying response function obtained in the time domain is approximated by a sum of decaying exponential functions, having the same form as in Eq. (14). We now show that this method can be applied to the Miki model of a semi-infinite ground layer.

Because $c_M = a_M \cot[(b_M+1)\pi/2]$ and $d_M = b_M$ [9], the impedance given by Eq. (1) can be rewritten

$$Z(\omega) = \rho_0 c_0 \left(1 + \frac{\mu}{(-j\omega)^{-b_M}}\right) \tag{22}$$

with

$$\mu = \frac{a_M}{(-2\pi\sigma_e j)^{b_M}} \left(1 + j\cot\frac{(b_M+1)\pi}{2}\right) = \frac{a_M}{(2\pi\sigma_e)^{b_M}} \left(\sin\frac{(b_M+1)\pi}{2}\right)^{-1} \tag{23}$$

The second equality of Eq. (23) shows that μ is real. Using Eq. (29.3.7) of [22], the following Fourier transform is found:

$$\mathcal{F}^{-1}\left[\frac{1}{(-j\omega)^{-b}}\right] = \frac{t^{-b-1}}{\Gamma(-b)} \tag{24}$$

Hence,

$$z(t) = \rho_0 c_0 \left[\delta(t) + \frac{\mu}{\Gamma(-b_M)} t^{-b_M-1} H(t)\right] \tag{25}$$

where $\delta(t)$ is the Dirac delta function. Then the slow decaying response function t^{-b_M-1} is approximated by a sum of decaying exponential functions:

$$t^{-b_M-1} \approx \sum_{k=1}^{S} A_k e^{-\lambda_k t} H(t) \tag{26}$$

Using Eq. (19), and taking into account the Dirac delta function in Eq. (25), the following TDBC is obtained:

$$p^{(n)} = \rho_0 c_0 \left[v^{(n)} + \sum_{k=1}^{S} A'_k \phi_k^{(n)}\right] \tag{27}$$

with $A'_k = A_k \mu / \Gamma(-b_M)$. The accumulator ϕ_k is updated using the recursive formula (20).

To obtain the same type of TDBC as in Ostashev et al. [15], another form of the recursive formula (20) is used:

$$\phi_k^{(n)} \approx v^{(n)} \Delta t + \phi_k^{(n-1)} e^{-\lambda_k \Delta t} \tag{28}$$

which assumes that $\lambda_k \Delta t$ is small. Equation (28) can be plugged into the TDBC of Eq. (27), which is then written

$$v^{(n)} = \frac{1}{1 + \Delta t \sum_{k=1}^{S} A'_k} \left[\frac{p^{(n)}}{\rho_0 c_0} - \sum_{k=1}^{S} A'_k e^{-\lambda_k \Delta t} \phi_k^{(n-1)}\right] \tag{29}$$

Equation (29) is very similar to Eq. (15) of Ostashev et al. [15] derived for the modified Zwikker and Kosten model.

It appears that Ostashev et al. [15] used the same template functions as Reymen et al. [14], considering real poles only. As will be seen in Sec. III.C, the main difference is that Reymen et al. [14] obtain the coefficients of the template functions by approximating the impedance in the frequency domain, whereas Ostashev et al. [15] obtain them by approximating the response functions in the time domain. Also, the latter approach can only be applied if the inverse Fourier transform of the impedance can be calculated analytically and thus cannot be applied to arbitrary impedance models.

Table 1 Errors err(Re[$Z(\omega)$]) and err(Im[$Z(\omega)$]) for the Miki impedance model of a semi-infinite ground layer ($\sigma_e = 100$ kPa · s · m^{-2}) using two coefficient identification methods in the frequency domain

Sets of coefficients	S	max($\lambda_k \Delta t$)[a]	err(Re[$Z(\omega)$])	err(Im[$Z(\omega)$])
VF S4	4	7.0	0.3%	0.2%
VF S5	5	13.3	0.1%	0.0%
VF S6	6	23.0	0.0%	0.0%
OF v1	5	5.0	0.5%	0.4%
OF v2	4	2.5	0.9%	0.7%

[a] $\Delta t = 1.47 \times 10^{-4}$ s.

C. Coefficient Identification Methods

1. Vector Fitting Approximation

The first coefficient identification method that is presented is the Vector Fitting (VF) technique proposed by Gustavsen and Semlyen [23]. This technique has been used by Reymen et al. [14] to identify the coefficients of Eqs. (13) and (15) in the frequency domain. VF is a powerful technique to fit calculated or measured frequency-dependent data with rational function approximation; the poles are guaranteed to be real and causal. It is an iterative method[¶] that generally converges on an optimum solution after a few iterations.

The VF technique is first applied to the Miki model of a semi-infinite ground layer. For this impedance model, VF yields only real poles if the number of poles is kept relatively small (less than 10). In Table 1, the errors err(Re[$Z(\omega)$]) and err(Im[$Z(\omega)$]) are given, where the error for the estimate X of the exact function X^{exact} is defined as

$$\text{err}\,(X) = \left[\sum_{m=1}^{N} (X_m - X_m^{\text{exact}})^2 \Big/ \sum_{m=1}^{N} (X_m^{\text{exact}})^2\right]^{1/2} \tag{30}$$

The estimates are obtained considering $N = 100$ frequencies logarithmically spaced between 50 and 1200 Hz, which corresponds to the frequency range covered by the numerical simulations presented in Sec. IV. It took a few seconds to obtain each of the estimates on a personal computer equipped with a Pentium 4 processor running at 3.2 GHz and with 2 GB of RAM memory. The impedance fit obtained with four poles, referred to as VF S4 in Table 1, is compared with the Miki model in Fig. 3 using a log–log scale. The fit and the model cannot be distinguished over the frequency band 50–1200 Hz. This result is confirmed by Table 1, where the errors are seen to be quite small using the VF technique, even when only four poles are considered. The maximum value of $\lambda_k \Delta t$ is also given in Table 1. A time step Δt of 1.47×10^{-4} s is used, corresponding to the largest time interval encountered in the simulations. The maximum value of $\lambda_k \Delta t$ increases rapidly with the number of real poles S. It will be shown in Sec. IV that this increase has an impact on the accuracy of the numerical calculations.

The VF method is then applied to the Miki model of a rigidly backed layer of thickness 0.01 m. When the total number of poles $S + 2T$ is greater than six, VF now yields complex poles as well as real poles, as can be seen in Table 2. The maximum value of $\beta_l \Delta t$ is seen to increase rapidly with the total number of poles.

2. Optimization in the Frequency Domain

It will be seen in Sec. IV that it is desirable to constrain the values of the coefficients λ_k. This cannot be done straightforwardly using the VF technique; thus, another coefficient identification method is proposed. It is based on a minimization procedure in the frequency

[¶] Data available only at http://www.energy.sintef.no/produkt/VECTFIT/index.asp [retrieved 22 July 2009].

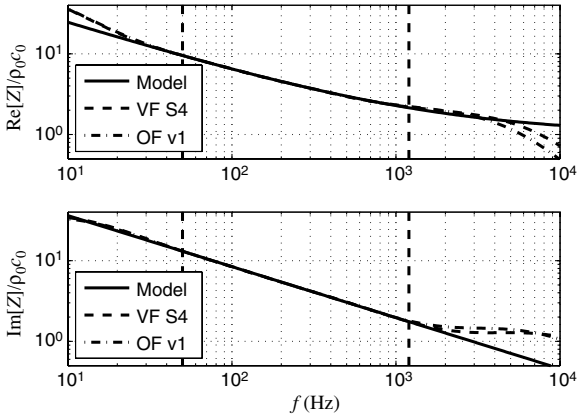

Fig. 3 Real and imaginary parts of the normalized impedance of a semi-infinite layer of effective flow resistivity 100 kPa · s · m^{-2}: Miki model (solid line), fit obtained with the set of coefficients VF S4 (dashed line), fit obtained with the set of coefficients OF V1 (dashed-dotted line), and frequency band 50–1200 Hz (vertical lines).

domain. Considering only real poles, the optimization in the frequency domain (OF) aims at finding the coefficients A_k and λ_k in the approximation

$$Z(\omega) \approx \sum_{k=1}^{S} \frac{A_k}{\lambda_k - j\omega} = \sum_{k=1}^{S} \frac{A_k \lambda_k}{\lambda_k^2 + \omega^2} + j \sum_{k=1}^{S} \frac{A_k \omega}{\lambda_k^2 + \omega^2} \tag{31}$$

Furthermore, the causality condition $\lambda_k \geq 0$ and the accuracy condition $\lambda_k \Delta t \leq L_{\text{thres}}$ are imposed, with L_{thres} as a threshold value. The optimization cannot be done using a simple minimization procedure, as it will be done in the time domain, because $Z(\omega)$ is complex. There are two functions to minimize, which are the real and imaginary parts of Eq. (31); this corresponds to a multiobjective optimization problem. This type of problem can be solved, for instance, using an ϵ-constraint method [24]. With the MATLAB function `fmincon` from the Optimization Toolbox, the function

$$\text{Re}\,[Z(\omega)] - \sum_{k=1}^{S} \frac{A_k \lambda_k}{\lambda_k^2 + \omega^2}$$

is minimized under the following constraints:

Constraint 1: $\lambda_k \geq 0$

Constraint 2: $\lambda_k \Delta t \leq L_{\text{thres}}$

Constraint 3:

$$\left| \text{Im}[Z(\omega)] - \sum_{k=1}^{S} \frac{A_k \omega}{\lambda_k^2 + \omega^2} \right| \leq \epsilon$$

where $\Delta t = 1.47 \times 10^{-4}$ s.

The two first sets of coefficients are obtained for the Miki model of a semi-infinite ground layer. In the first optimization that is performed, 100 frequencies logarithmically spaced between 50 and 1200 Hz are considered, and L_{thres} is set to five. A number of 100 optimizations with random values of A_k and λ_k are performed with a relatively large value of ϵ, equal to $\min(\text{Im}[Z(\omega)])/5$. The initial random values of A_k and λ_k are chosen between zero and $1/\Delta t$. A set of coefficients that yields small values of the errors $\text{err}(\text{Re}[Z(\omega)])$ and $\text{err}(\text{Im}[Z(\omega)])$ is selected. Then, additional optimizations are performed with smaller values of ϵ until a good approximation of the real and imaginary parts of the impedance is obtained. The results associated with this first optimization, noted OF v1, are given in Table 1 and the associated fit is plotted in Fig. 3. The second optimization, noted OF v2, is performed in a similar way, considering 100 frequencies logarithmically spaced between 50 and 600 Hz; L_{thres} is reduced to 2.5.

Two sets of coefficients are also obtained for the Miki model of a rigidly backed layer of thickness 0.01 m following the same procedure. The first optimization, noted OF v1L, is performed on the frequency range 50–1200 Hz with a threshold value of 5, and the second optimization, noted OF v2L, is performed in the frequency range 50–600 Hz with a threshold value of 2.5. The results associated with these sets of coefficients are given in Table 2. Each optimization process took about 20 min to run on the same computer as the one used in Sec. III.C.1. Compared with the vector fitting technique, the optimization in the frequency domain is more time-consuming because the initial values of A_k and λ_k in the algorithm are chosen randomly. However, once a good choice of initial values of A_k and λ_k has been selected, it is quite fast and efficient to perform the additional optimizations yielding the desired sets of coefficients.

3. *Optimization in the Time Domain*

The third and last method of coefficient identification that is described is based on Eq. (26), corresponding to the Miki model of a semi-infinite ground layer. An optimization procedure is used to minimize the difference between the left and right hand sides of Eq. (26). This optimization in the time domain (OT) is performed over the range $0 \leq t \leq 100$ ms, with a time step of 0.1 ms. As done in the optimization method in the frequency domain, 100 optimizations with random values of A_k and λ_k are performed, and then a set of coefficients that yields a small value of the error $\text{err}(t^{-b_M-1})$ is selected. First, following Ostashev et al. [15], the optimization procedure is based on the MATLAB function `fminsearch`. This corresponds to an *unconstrained nonlinear optimization*, because there is no constraint on the values of A_k and λ_k. This first optimization is referred to as OT v1 in Table 3. Second, the MATLAB function `fmincon` is used to perform the optimization with the additional constraint $\lambda_k \Delta t \leq 1$. With this second optimization, noted OT v2, the error in the approximation of the response function t^{-b_M-1} is larger than with OT v1. Each optimization process took about 50 min to run on the same computer as the one used in Sec. III.C.1. Compared with the optimization method in the frequency domain, the computation time is greater because of the large number of time samples considered here (1000 time samples) with respect to

Table 3 Error $\text{err}(t^{-b_M-1})$ for the Miki impedance model of a semi-infinite ground layer (σ_e = 100 kPa · s · m^{-2}) using the coefficient identification method in the time domain

Sets of coefficients	S	$\max(\lambda_k \Delta t)$[a]	$\text{err}(t^{-b_M-1})$[a]
OT v1	6	1.3	0.3%
OT v2	6	0.4	1.0%

[a]$\Delta t = 1.47 \times 10^{-4}$ s

Table 2 Errors $\text{err}(\text{Re}[Z(\omega)])$ and $\text{err}(\text{Im}[Z(\omega)])$ for the Miki impedance model of a rigidly backed layer of thickness 0.01 m (σ_e = 100 kPa · s · m^{-2}) using two coefficient identification methods in the frequency domain

Sets of coefficients	S	$\max(\lambda_k \Delta t)$[a]	T	$\max(\alpha_l \Delta t)$[a]	$\max(\beta_l \Delta t)$[a]	$\text{err}(\text{Re}[Z(\omega)])$	$\text{err}(\text{Im}[Z(\omega)])$
VF S4T1L	4	0.8	1	5.5	3.2	1.5%	0.1%
VF S6T1L	6	0.7	1	4.9	6.3	0.1%	0.0%
VF S8T1L	8	0.9	1	0.4	11.5	0.1%	0.0%
OF v1L	6	4.7	0	——	——	0.6%	0.0%
OF v2L	6	2.1	0	——	——	0.3%	0.0%

[a]$\Delta t = 1.47 \times 10^{-4}$ s

the number of frequency samples used in Sec. III.C.2 (100 frequency samples).

IV. Numerical Results Using the Linearized Euler Equations

A. Linearized Euler Equation Solver

The LEE are solved in the time domain using low-dispersion and low-dissipation explicit numerical schemes developed in the computational aeroacoustics community, and also used for turbulence simulations [25]. Optimized finite difference schemes and selective filters over 11 points are used for spatial derivation and grid-to-grid oscillations removal, respectively. These schemes allow accurate calculation of acoustic wavelengths down to approximately five times the spatial mesh size. For the interior points, the points separated from the boundary by at least five points, the centered fourth-order finite difference scheme of Bogey and Bailly [26] and the centered sixth order selective filter recently proposed by Bogey et al. [27] are chosen. For the boundary points, the five extreme points in each direction, the 11-point noncentered finite difference schemes and selective filters of Berland et al. [28] are used. Applying a selective filter to a variable U on a uniform mesh of size Δx provides

$$U^f(x_0) = U(x_0) - s_f \sum_{m=-P}^{Q} d_m U(x_0 + m\Delta x) \tag{32}$$

In the following, a filtering coefficient s_f of 0.2 is taken for all selective filters except at the extreme points where no filtering is applied. The optimized six-stage Runge–Kutta algorithm proposed by Bogey and Bailly [26] is used for time integration. It only uses two storage locations per variable and has a high stability limit. For the differential equation

$$\frac{\partial U}{\partial t} = F(U) \tag{33}$$

the explicit p-stage Runge–Kutta algorithm advances the solution from the nth to the $(n+1)$th iteration as [26]

$$U^{(0)} = U^{(n)} \tag{34a}$$

$$U^{(i)} = U^{(n)} + \gamma_i \Delta t K_U, \qquad i = 1 \ldots p \tag{34b}$$

$$U^{(n+1)} = U^{(p)} \tag{34c}$$

where $K_U = F(U^{(i-1)})$ in Eq. (34b). The simulations presented in this paper are obtained with a Courant–Friedrichs–Lewy (CFL) $c_0 \Delta t / \Delta x$ of 1.

The TDBC described in Sec. III can easily be adapted to this Runge–Kutta algorithm, noting that the time step between two consecutive stages is taken as $(\gamma_i - \gamma_{i-1})\Delta t$. For the frequency-domain approximation, the following steps are implemented at stage i for the points at the boundary:

1) Advance v in time following Eq. (34b): $v^{(i)} = v^{(n)} + \gamma_i \Delta t K_v$.
2) Advance ϕ_k and ψ_l in time using Eqs. (20) and (21):

$$\phi_k^{(i)} = v^{(i)} \frac{1 - e^{-\lambda_k(\gamma_i - \gamma_{i-1})\Delta t}}{\lambda_k} + \phi_k^{(i-1)} e^{-\lambda_k(\gamma_i - \gamma_{i-1})\Delta t}$$

$$\psi_l^{(i)} = v^{(i)} \frac{1 - e^{-(\alpha_l - j\beta_l)(\gamma_i - \gamma_{i-1})\Delta t}}{\alpha_l - j\beta_l} + \psi_l^{(i-1)} e^{-(\alpha_l - j\beta_l)(\gamma_i - \gamma_{i-1})\Delta t}$$

3) Calculate K_p using Eq. (19) and (34b):

$$K_p = \frac{1}{\gamma_i \Delta t}\left[\sum_{k=1}^{S} A_k \phi_k^{(i)} + \sum_{l=1}^{T}\left(C_l \,\mathrm{Re}[\psi_l^{(i)}] + \frac{D_l - \alpha_l C_l}{\beta_l}\,\mathrm{Im}[\psi_l^{(i)}]\right) - p^{(n)}\right]$$

4) Advance p in time following Eq. (34b): $p^{(i)} = p^{(n)} + \gamma_i \Delta t K_p$.

For the time-domain approximation, the following steps are implemented at stage i for the points at the boundary:

1) Advance p in time following Eq. (34b): $p^{(i)} = p^{(n)} + \gamma_i \Delta t K_p$.
2) Calculate K_v using Eq. (29) and (34b):

$$K_v = \frac{1}{\gamma_i \Delta t}\left(\frac{p^{(i)}/\rho_0 c_0 - \sum_{k=1}^{S} A'_k e^{-\lambda_k(\gamma_i - \gamma_{i-1})\Delta t}\phi_k^{(i-1)}}{1 + (\gamma_i - \gamma_{i-1})\Delta t \sum_{k=1}^{S} A'_k} - v^{(n)}\right)$$

3) Advance v in time following Eq. (34b): $v^{(i)} = v^{(n)} + \gamma_i \Delta t K_v$.
4) Advance ϕ_k in time using Eq. (28):

$$\phi_k^{(i)} = v^{(i)}(\gamma_i - \gamma_{i-1})\Delta t + \phi_k^{(i-1)} e^{-\lambda_k(\gamma_i - \gamma_{i-1})\Delta t}$$

These are two ways to implement the time-domain boundary conditions, but other implementations could also be considered.

In the numerical simulations, the initial pressure distribution at $t = 0$ has a Gaussian form. In 1-D,

$$p(x, t=0) = \exp\left(-\ell n\, 2 \frac{x^2}{B^2}\right) \tag{35}$$

where B is the Gaussian half-width. The shape of the Gaussian pulse and its frequency content are plotted in Fig. 4 for $B = 3\Delta x$ and $B = 5\Delta x$. To avoid spurious reflections, the source should be located at least $10\Delta x$ away from a boundary if $B = 3\Delta x$, and $15\Delta x$ away from a boundary if $B = 5\Delta x$. In the one- and three-dimensional test cases presented in Secs. IV.B and IV.C , the mesh size Δx is set to 0.05 m or 0.10 m. Figure 4 shows that the pulse has a significant frequency content for $k_x \Delta x$ approximately between zero and $3\pi/8$ with $B = 3\Delta x$. The upper limit $k_x \Delta x = 3\pi/8$ corresponds to a frequency of 1280 Hz if $\Delta x = 0.05$ m or 640 Hz if $\Delta x = 0.10$ m. With $B = 5\Delta x$, the upper limit is reduced to approximately $k_x \Delta x = \pi/4$, which corresponds to a frequency of 850 Hz if $\Delta x = 0.05$ m or 430 Hz if $\Delta x = 0.10$ m.

For the three-dimensional simulations of Secs. IV.C and IV.D, the radiation boundary conditions derived by Bogey and Bailly [29] are

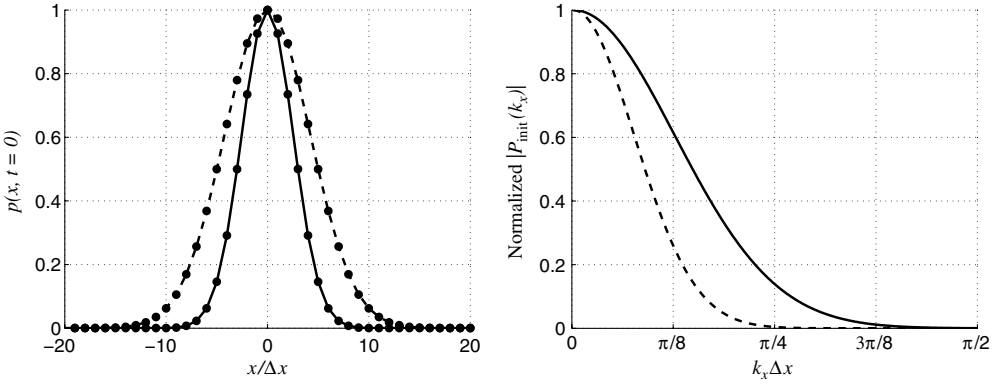

Fig. 4 Gaussian initial pressure pulse $p(x, t = 0)$ (left) and its normalized magnitude spectrum $|P_{\mathrm{init}}(k_x)|$ (right) with a Gaussian half-width $B = 3\Delta x$ (solid line) or $B = 5\Delta x$ (dashed line).

used; they are an extension of Tam and Dong's [30] work in a two-dimensional geometry. These boundary conditions are applied to the last three rows of points at each boundary except at the impedance boundary. The origin used for the radiation boundary conditions is located on the ground.

B. One-Dimensional Test Cases

Consider a one-dimensional propagation test case, with an impedance boundary condition on the left ($x = 0$) and a radiation boundary condition on the right. The computational domain has a length of 101 points and the Gaussian pressure distribution is initially located at the center of the domain. First, a perfectly reflecting boundary condition is placed on the left of the domain. Results are given in terms of nondimensional variables because they are independent on the mesh size. In particular, let $\bar{t} = t/(\Delta x/c_0)$ be the normalized time. Two pressure distributions at $\bar{t} = 20$ and $\bar{t} = 140$ are plotted in Fig. 5. At $\bar{t} = 20$, the left- and right-traveling waves are in the computational domain. The right-traveling wave is exiting the domain at about $\bar{t} = 50$, whereas the left-traveling wave is reflected by the wall. At $\bar{t} = 140$, the reflected wave is then close to the limit of the domain. The error rate is defined as

$$e_{\text{num}} = \left[\sum_{m=1}^{N_x}(p_m^{\text{num}} - p_m^{\text{exact}})^2 \Big/ \sum_{m=1}^{N_x}(p_m^{\text{exact}})^2\right]^{1/2} \tag{36}$$

where $N_x = 101$ is the number of points in the domain, p^{num} is the numerical solution, and p^{exact} is the analytical solution. In Fig. 6, the dashed curve corresponds to the plot of the error rate with respect to the normalized time $\bar{t}$ for the perfectly reflecting wall. In testing, it has been found that by increasing the length of the domain, the error due to the radiation boundary condition is very small. Over a perfectly reflecting ground,

$$\max_{\bar{t}\le 140}[e_{\text{num}}] = \begin{cases} 0.3\% & \text{for } B = 5\Delta x, \\ 0.9\% & \text{for } B = 3\Delta x \end{cases} \tag{37}$$

These values can be considered as a lower bound for the error rate.

Consider now an impedance TDBC on the left of the domain. The analytical solution p^{exact} that appears in Eq. (36) is calculated by inverse Fourier transform of the frequency-domain solution, as proposed by Rienstra [31]. First, the Miki model for a semi-infinite ground layer with an effective flow resistivity of 100 kPa · s · m^{-2} is considered. The error rates are given in Table 4 for the sets of coefficients obtained using the two methods in the frequency domain (see Table 1), and the method in the time domain (see Table 3). Using the vector fitting approximation, it appears that the error rate increases with the number of poles, whereas the impedance is better approximated with a greater number of poles as seen in Table 1. This unexpected behavior is also illustrated in Fig. 6, in which the error rates are plotted with respect to the normalized time for a mesh size of 0.05 m. This result can be explained by the values of the poles λ_k. In the context of electromagnetic propagation through dispersive media, it is common to approximate the complex permittivity with a sum of single-pole systems; this is referred to as Debye function expansion [32]. Several authors, including Young et al. [33], Beck and Mirotznik [34], and Kelley et al. [32], have shown that the time step Δt must be small compared with all the time scales of the problem, including $1/\lambda_k$, to accurately represent the problem. In Table 1, the maximum of $\lambda_k \Delta t$ is seen to increase from seven to 23 when the number of real poles S goes from four to six in the VF algorithm, which explains the increase of the error rate with S. A value of Δt of 1.47×10^{-4} s is used in Tables 1–3, which corresponds to $\Delta x = 0.10$ m, taking into account that the maximum of $(\gamma_i - \gamma_{i-1})$ is 0.5 with the Runge–Kutta algorithm used in the solver [26]. For a mesh size of 0.05 m, the time step is twice as small, and the error is expected to be somewhat smaller. For instance, with

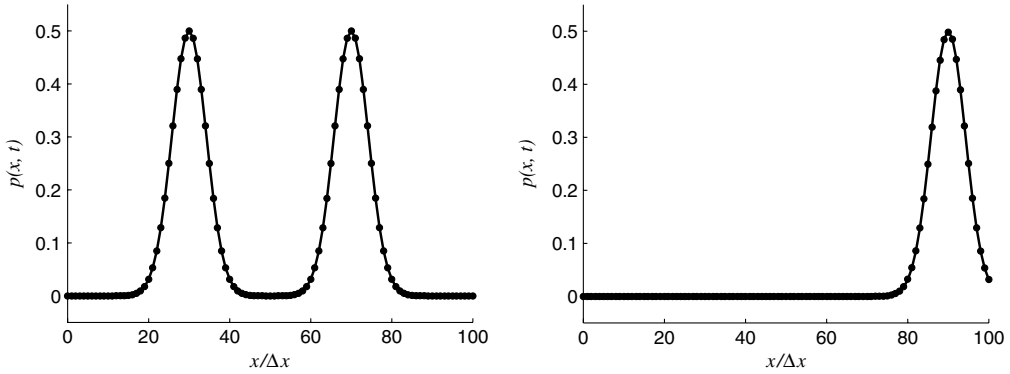

Fig. 5 Pressure distributions for the analytical solution (solid line) and the numerical solution (dots) at the normalized times $\bar{t} = 20$ (left) and $\bar{t} = 140$ (right). A perfectly reflecting boundary condition is placed at $x = 0$, and the Gaussian half-width is $B = 5\Delta x$.

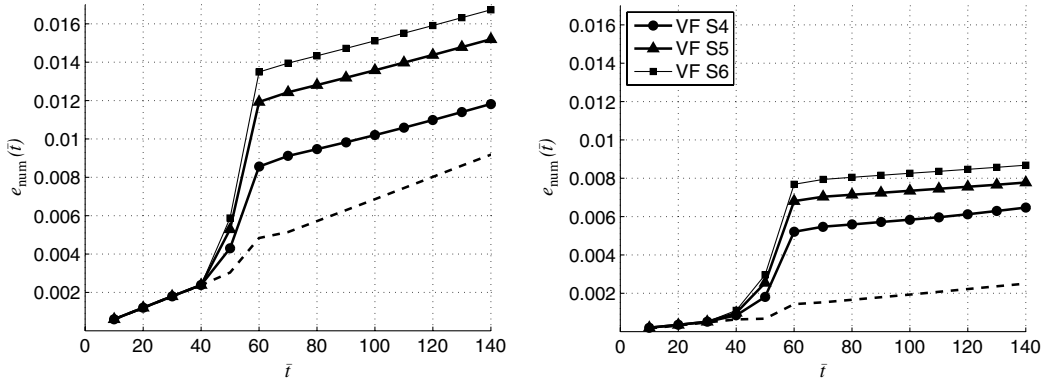

Fig. 6 Error rates obtained with the Miki impedance model of a semi-infinite ground layer ($\sigma_e = 100$ kPa · s · m^{-2}) using the vector fitting technique with 4 poles (circles), 5 poles (triangles), and 6 poles (squares); perfectly reflecting ground case (dashed line); Gaussian half-width is $B = 3\Delta x$ (left) or $B = 5\Delta x$ (right) with $\Delta x = 0.05$ m.

Table 4 One-dimensional test case results for the Miki impedance model of a semi-infinite ground layer ($\sigma_e = 100$ kPa · s · m^{-2}) using the sets of coefficients described in Tables 1 and 3

	$\max[e_{\text{num}}]$ with $B = 3\Delta x$			$\max[e_{\text{num}}]$ with $B = 5\Delta x$	
Sets of coefficients	$\Delta x = 0.05$ m	$\Delta x = 0.10$ m	Sets of coefficients	$\Delta x = 0.05$ m	$\Delta x = 0.10$ m
VF S4	1.2%	1.2%	VF S4	0.6%	0.8%
VF S5	1.5%	1.5%	VF S5	0.8%	0.8%
VF S6	1.7%	2.0%	VF S6	0.9%	1.1%
OF v1	0.9%	1.2%	OF v1	0.6%	0.8%
OF v2	——	0.8%	OF v2	——	0.8%
OT v1	1.0%	1.1%	OT v1	0.7%	0.7%
OT v2	1.7%	0.6%	OT v2	1.1%	0.4%

Table 5 One-dimensional test case results for the Miki impedance model of a rigidly backed layer of thickness 0.01 m ($\sigma_e = 100$ kPa · s · m^{-2}) using the sets of coefficients described in Table 2

	$\max[e_{\text{num}}]$ with $B = 3\Delta x$			$\max[e_{\text{num}}]$ with $B = 5\Delta x$	
Sets of coefficients	$\Delta x = 0.05$ m	$\Delta x = 0.10$ m	Sets of coefficients	$\Delta x = 0.05$ m	$\Delta x = 0.10$ m
VF S4T1L	1.0%	1.1%	VF S4T1L	0.5%	0.5%
VF S6T1L	1.2%	1.4%	VF S6T1L	0.6%	0.5%
VF S8T1L	Unstable	Unstable	VF S8T1L	Unstable	Unstable
OF v1L	0.8%	1.0%	OF v1L	0.4%	0.5%
OF v2L	——	0.8%	OF v2L	——	0.3%

the set of coefficients VF S6 and a Gaussian half-bandwidth $B = 3\Delta x$, the error rate is 1.7% with $\Delta x = 0.05$ m and 2.0% with $\Delta x = 0.10$ m.

In the optimization method in the frequency domain, an accuracy condition $\lambda_k \Delta t \leq L_{\text{thres}}$ has been added to constrain the value of the coefficients λ_k. For the set of coefficients OF v1, obtained over the frequency range 50–1200 Hz with $L_{\text{thres}} = 5$, small values of the error rate are found, especially when a mesh size of 0.05 m is used with error rates of 0.9% with $B = 3\Delta x$ and of 0.6% with $B = 5\Delta x$. The set of coefficients OF v2 is obtained over the frequency range 50–600 Hz with $L_{\text{thres}} = 2.5$; thus, the error rates are only calculated with a mesh size of 0.10 m, at which most of the energy is below 600 Hz. The optimization OF v2 yields an error rate of 0.8% for the two half-bandwiths considered. Finally, results for the optimization in the time domain are given in Table 4. The set of coefficients OT v1, obtained using an unconstrained optimization procedure, performs well with a mesh size of 0.05 m, with error rates $\leq 1.0\%$. On the other hand, the optimization OT v2, obtained with the constraint $\lambda_k \Delta t \leq 1$, yields small error rates with $\Delta x = 0.10$ m equal to 0.6% with $B = 3\Delta x$ and equal to 0.4% with $B = 5\Delta x$. Generally speaking, the results for the sets of coefficients OF and OT show that a trade-off must be found between the quality of the fit of the impedance $Z(\omega)$ or the response function $z(t)$ and the constraint on the maximum value of $\lambda_k \Delta t$.

The Miki model for a rigidly backed layer of thickness 0.01 m and effective flow resistivity 100 kPa · s · m^{-2} is now considered. The error rates are given in Table 5 for the sets of coefficients obtained with the two methods in the frequency domain (see Table 2). The role of complex conjugated poles is investigated using the sets of coefficients obtained by vector fitting. The error rates are seen to be higher when the total number of poles $S + 2T$ goes from six to eight. This can be explained by the increase of the maximum value of $\beta_l \Delta t$, as seen in Table 2. As mentioned before, the time step Δt must be small compared with all time scales to accurately represent the problem. When complex conjugated poles are used, this means that not only $\lambda_k \Delta t$ but also $\alpha_l \Delta t$ and $\beta_l \Delta t$ must be small to keep a good accuracy. With the set of coefficients VF S8T1L, including 10 poles, the calculations become unstable, which seems to be linked with the large value of $\beta_l \Delta t$ obtained with these coefficients. This stability issue has been studied by Beck and Mirotznik [34] in the context of electromagnetic propagation through dispersive media. For second-order systems (complex conjugated poles), also referred to as Lorentz media, Beck and Mirotznik [34] showed that the calculations are not unconditionally stable, and that it might be necessary to reduce the time step to maintain stability. Finally, using the optimization method in the frequency domain, small error rates are obtained. The set of coefficients OF v1L is better suited to calculations with a mesh size of 0.05 m, whereas the set OF v2L performs better with a mesh size of 0.10 m. These two sets of coefficients yield error rates $\leq 0.8\%$ with $B = 3\Delta x$ and $\leq 0.4\%$ with $B = 5\Delta x$.

C. Three-Dimensional Test Cases

Consider now a three-dimensional propagation test case, with an impedance boundary condition on the bottom ($z = 0$) and radiation boundary conditions at the other limits of the domain. The initial Gaussian pulse is located at $(x_S, y_S, z_S) = (0, 0, 20\Delta x)$; this value of the source height z_S ensures that the entire pulse is in the computational domain (see Fig. 4). The computation domain must be sufficiently large so that the error introduced by the radiation boundary conditions is small; thus, the size of the domain is set to $201 \times 201 \times 201$ points, but the error rate will be calculated over a subdomain of $101 \times 101 \times 101$ points. First, the acoustic propagation over a perfectly reflecting ground is studied to define a criterion for the error; the results are independent of the mesh size Δx in that case. Pressure contours in the $y = 0$ plane are plotted in Fig. 7 at the normalized times $\bar{t} = 40$ and $\bar{t} = 120$. The error rate e_{num} is estimated over a volume of $101 \times 101 \times 101$ points, the limit of which are represented by dashed lines in Fig. 7, extending the formula of Eq. (36). Note that the pressure contours calculated analytically and plotted with dotted lines in Fig. 7 cannot be distinguished from the pressure contours calculated numerically and plotted with solid lines. At $\bar{t} = 120$, the reflected wave is about to leave the volume over

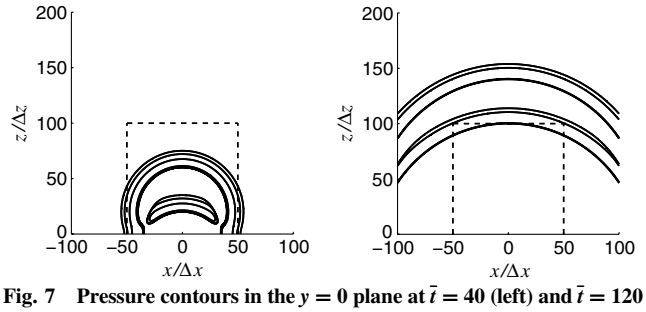

Fig. 7 Pressure contours in the $y = 0$ plane at $\bar{t} = 40$ (left) and $\bar{t} = 120$ (right) for the perfectly reflecting ground case, using a Gaussian half-width $B = 5\Delta x$. Pressure isocontours 2.5×10^{-4}, 2×10^{-3}, and 1.6×10^{-2} are plotted for the numerical solution (solid line) and the analytical solution (dotted line); the numerical and analytical solutions cannot be distinguished on these plots.

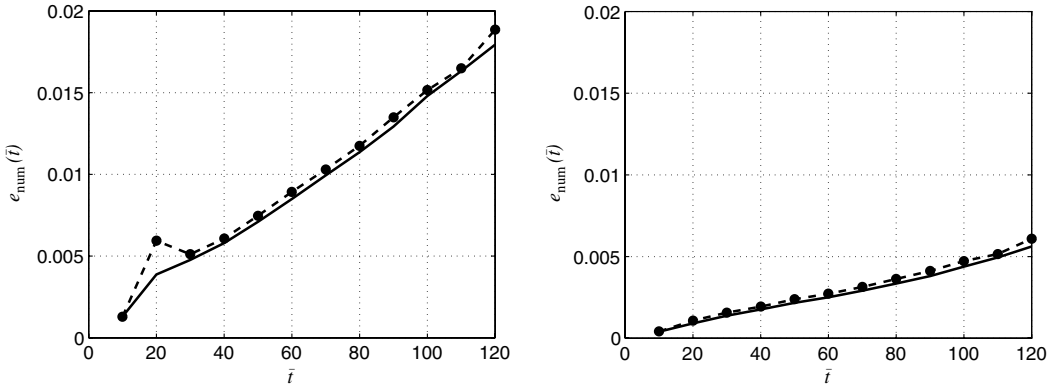

Fig. 8 Error rates for the perfectly reflecting ground case, using a Gaussian half-width $B = 3\Delta x$ (left) and $B = 5\Delta x$ (right). The error rate is calculated over a volume of 101 × 101 × 101 points (solid line) and over the $y = 0$ plane of this volume (dashed line with circles).

which the error rate is calculated. This calculation of the error rate is represented as a solid line in Fig. 8. It requires the analytical solution to be known over approximately one million points. Over an impedance ground, the analytical solution in the time domain is calculated using the method proposed by Zheng and Zhuang [35]. This method uses a decomposition of the broadband spherical wave into harmonic spherical waves by Fourier transform in a first step, and a decomposition into harmonic plane waves using Weyl's integral [36] in a second step. A high computational effort is required to compute this analytical solution. Thus, the analytical solution cannot be obtained in the whole volume in a reasonable amount of time. To reduce the computational burden, the error rate is calculated over the 101×101 points of the $y = 0$ plane only, and is noted $e_{\text{num}}(y = 0)$. Figure 7 shows that the error rates calculated over the whole volume and over the $y = 0$ plane are very similar. As a result, the maximum of the error rate $e_{\text{num}}(y = 0)$ over $\bar{t} \leq 120$ will be the criterion used to assess the quality of the TDBC derived. Over a perfectly reflecting ground,

$$\max_{\bar{t}\leq 120}[e_{\text{num}}(y=0)] = \begin{cases} 0.6\% & \text{for } B = 5\Delta x, \\ 1.9\% & \text{for } B = 3\Delta x \end{cases} \tag{38}$$

The results for the Miki model of a semi-infinite ground layer with an effective flow resistivity of 100 kPa · s · m^{-2} are given in Table 6 for the same sets of coefficients as in Sec. IV.B. The trends obtained with the one-dimensional test case are confirmed. Using the VF algorithm, the error rate is quite large and increases when the number of poles goes from four to six due to the increase of the maximum value of $\lambda_k \Delta t$. The sets of coefficients OF v1 and OT v1 yield the best results using a mesh size of 0.05 m, with error rates $\leq 1.7\%$ with $B = 3\Delta x$ and $\leq 1.1\%$ with $B = 5\Delta x$. The sets OF v2 and OT v2 are better suited for the calculations using a mesh size of 0.10 m, with error rates $\leq 1.1\%$ with $B = 3\Delta x$ and $\leq 0.6\%$ with $B = 5\Delta x$. Error rates are seen to be generally higher with $B = 3\Delta x$ than with $B = 5\Delta x$, which can be attributed to the larger frequency range covered by the Gaussian distribution of smaller half-bandwith.

The results for the Miki model of a rigidly backed layer of thickness 0.01 m and effective flow resistivity 100 kPa · s · m^{-2} are given in Table 7 for the same sets of coefficients as in Sec. IV.B. As seen in the one-dimensional test case, the calculations with the set of coefficients VF S8T1L are unstable due to the large maximum value of $\beta_l \Delta t$. With a mesh size of 0.05 m, the set OF v1L performs the best, with error rates of 1.4% with $B = 3\Delta x$ and of 1.2% with $B = 5\Delta x$. Error rates obtained with a mesh size of 0.10 m are close for the sets of coefficients VF S4T1L, OF v1L and OF v2L. For this mesh size, the set OF v2L will be chosen in the following because of its small maximum value of $\lambda_k \Delta t$.

The numerical solution is now compared with the analytical solution in the frequency domain; this analytical solution is calculated using the classical expression for the reflection of a spherical wave from a locally reacting plane surface that can be found, for

Table 6 Three-dimensional test case results for the Miki impedance model of a semi-infinite ground layer ($\sigma_e = 100$ kPa · s · m^{-2}) using the sets of coefficients described in Tables 1 and 3

	$\max[e_{\text{num}}(y=0)]$ with $B = 3\Delta x$			$\max[e_{\text{num}}(y=0)]$ with $B = 5\Delta x$	
Sets of coefficients	$\Delta x = 0.05$ m	$\Delta x = 0.10$ m	Sets of coefficients	$\Delta x = 0.05$ m	$\Delta x = 0.10$ m
VF S4	2.2%	2.2%	VF S4	1.4%	1.3%
VF S5	3.0%	2.7%	VF S5	1.8%	1.7%
VF S6	3.3%	3.8%	VF S6	2.0%	2.5%
OF v1	1.7%	2.1%	OF v1	1.1%	1.3%
OF v2	——	1.1%	OF v2	——	0.6%
OT v1	1.5%	2.0%	OT v1	1.1%	1.2%
OT v2	3.0%	1.0%	OT v2	2.1%	0.6%

Table 7 Three-dimensional test case results for the Miki impedance model of a rigidly backed layer of thickness 0.01 m ($\sigma_e = 100$ kPa · s · m^{-2}) using the sets of coefficients described in Table 2

	$\max[e_{\text{num}}(y=0)]$ with $B = 3\Delta x$			$\max[e_{\text{num}}(y=0)]$ with $B = 5\Delta x$	
Sets of coefficients	$\Delta x = 0.05$ m	$\Delta x = 0.10$ m	Sets of coefficients	$\Delta x = 0.05$ m	$\Delta x = 0.10$ m
VF S4T1L	1.7%	2.1%	VF S4T1L	1.4%	1.8%
VF S6T1L	2.2%	2.3%	VF S6T1L	1.6%	1.8%
VF S8T1L	Unstable	Unstable	VF S8T1L	Unstable	Unstable
OF v1L	1.4%	1.9%	OF v1L	1.2%	1.8%
OF v2L	——	2.1%	OF v2L	——	1.7%

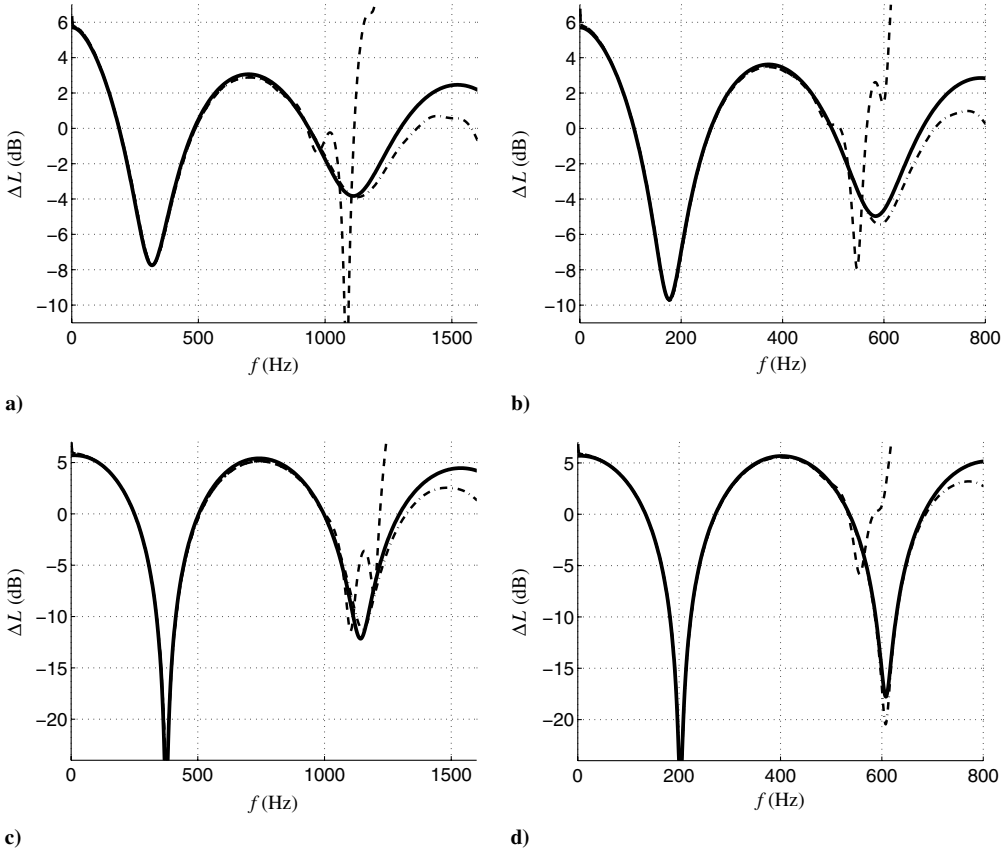

Fig. 9 Spectra of the sound pressure level relative to the free field ΔL at $x = 100\Delta x$, $y = 0$, and $z = z_S$; analytical solution (thick lines), numerical solution with $B = 3\Delta x$ (thin dashed-dotted lines), and numerical solution with $B = 5\Delta x$ (thin dashed lines); impedance of the semi-infinite ground layer (top) and impedance of the rigidly backed layer of thickness 0.01 m (bottom): a) OF v1 with $\Delta x = 0.05$ m, b) OF v2 with $\Delta x = 0.10$ m, c) OF v1L with $\Delta x = 0.05$ m, and d) OF v2L with $\Delta x = 0.10$ m.

instance, in Chessell [17]. Using a fast Fourier transform, the spectrum of the sound pressure level relative to the free field, noted ΔL, is calculated and compared with the analytical solution in Fig. 9 for the semi-infinite ground layer and for the rigidly backed layer of thickness 0.01 m. The sets of coefficients OF are used in the TDBC; these coefficients are given in the Appendix. The receiver is located at $x = 100\Delta x$, $y = 0$, and $z = z_S$ and thus at $x = 5$ m and $z = 1$ m for a mesh size of 0.05 m and at $x = 10$ m and $z = 2$ m for a mesh size of 0.10 m. For a mesh size of 0.05 m, the numerical solution follows the analytical solution well up to about 1000 Hz with $B = 5\Delta x$, and 1300 Hz with $B = 3\Delta x$. For a mesh size of 0.10 m, these frequency limits are reduced to about 500 Hz for $B = 5\Delta x$ and 700 Hz for $B = 3\Delta x$. These values are in agreement with those obtained in Sec. IV.A from the spectral shape of the initial Gaussian pulse, and show the broadband nature of the time-domain simulations presented.

D. A More Realistic Configuration for Outdoor Sound Propagation

In this section, a three-dimensional configuration with a preferred direction of propagation x is considered; this is a more realistic geometry for outdoor sound propagation calculations [37,38]. A mesh size Δx of 0.10 m is considered, the Gaussian half-width is $B = 3\Delta x$, and the source height is $20\Delta x = 2$ m. The sets of

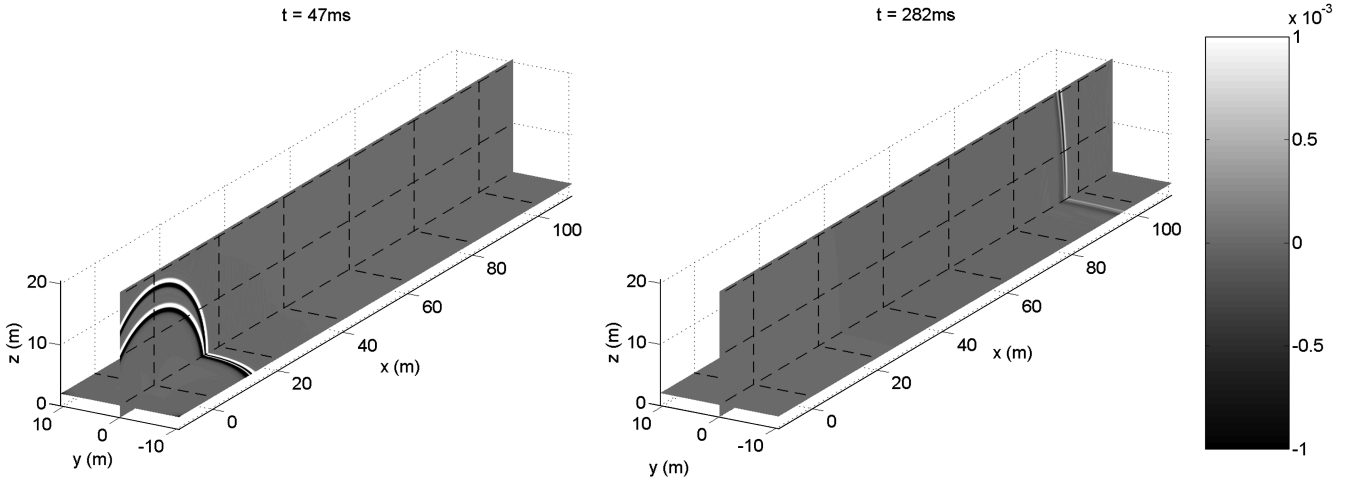

Fig. 10 Pressure maps on the $y = 0$ and $z = z_S$ planes after 160 iterations ($t = 47$ ms) and 960 iterations ($t = 282$ ms). The impedance of the semi-infinite ground layer is approximated by the set of parameters OF v2.

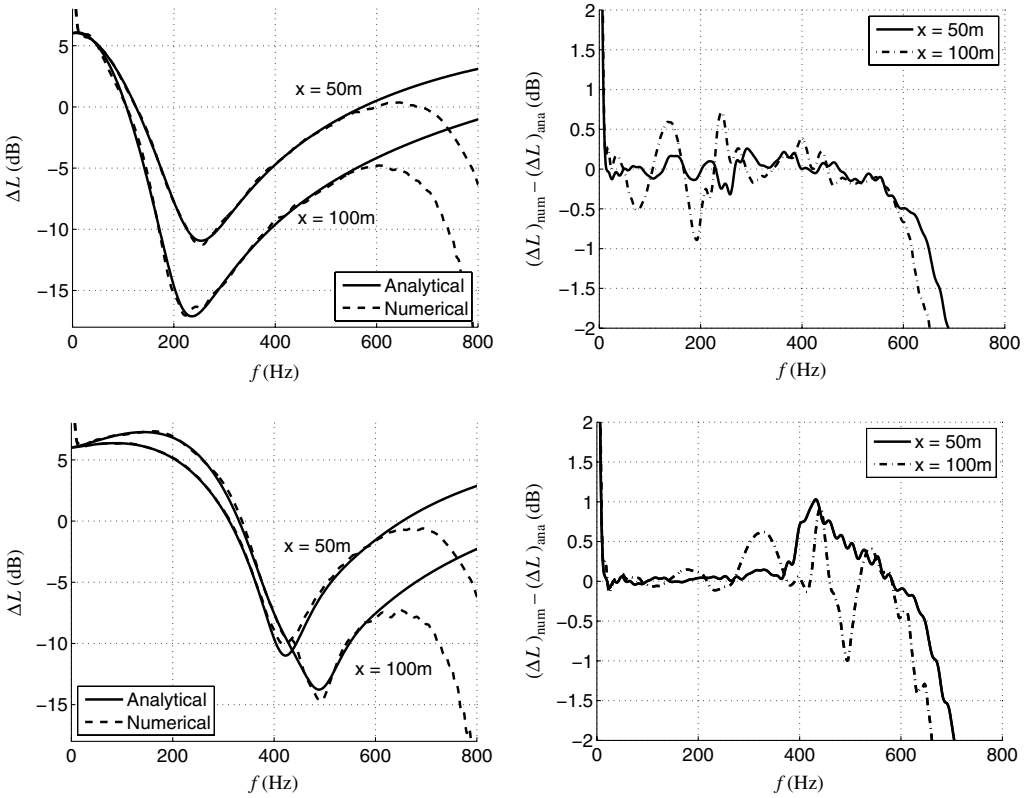

Fig. 11 On the left plots, the spectra of the sound pressure level relative to the free field ΔL are plotted for the analytical solution (solid line) and the numerical solution (dashed line). On the right plots, the spectra of the difference $(\Delta L)_{\text{num}} - (\Delta L)_{\text{ana}}$ between both solutions are plotted; $y = 0$ and $z = z_S$; the impedance of the semi-infinite ground layer is approximated by the set of parameters OF v2 (top) and the impedance of the rigidly backed layer of thickness 0.01 m is approximated by the set of parameters OF v2L (bottom).

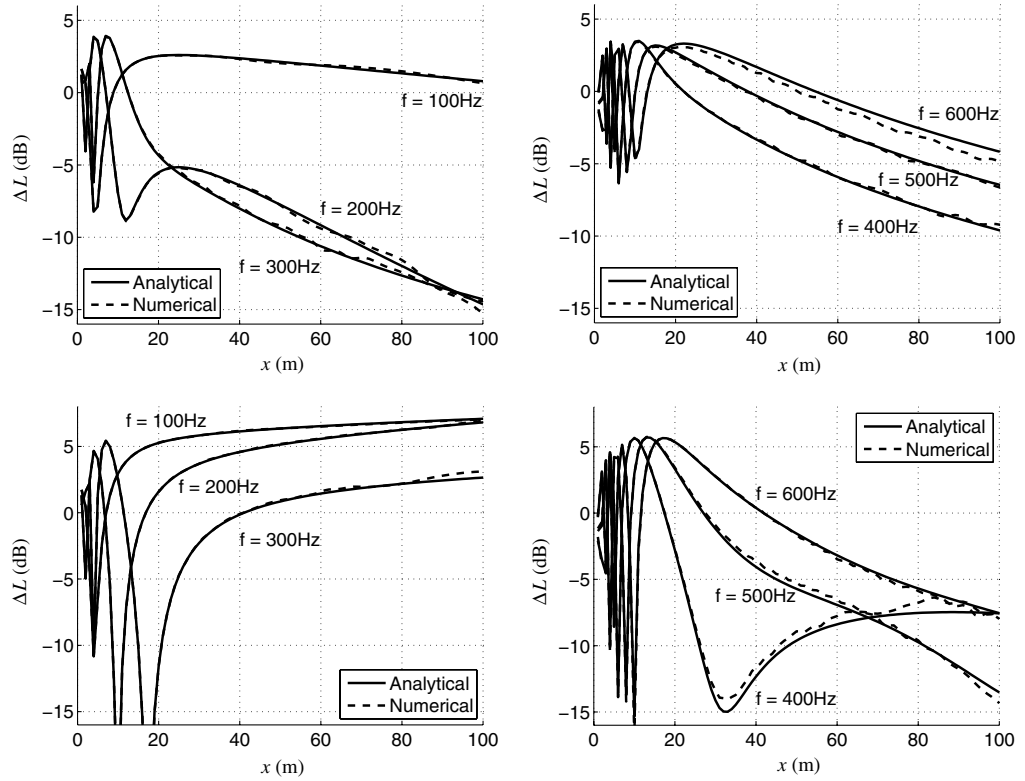

Fig. 12 Sound pressure level relative to the free field with respect to propagation distance x at $y = 0$ and $z = z_S$, and for different frequencies (as labeled); impedance of the semi-infinite ground layer is approximated by the set of parameters OF v2 (top) and impedance of the rigidly backed layer of thickness 0.01 m is approximated by the set of parameters OF v2L (bottom).

coefficients OF v2 and OF v2L are used in the TDBC relative to the Miki impedance model of a semi-infinite ground layer and of a rigidly backed layer of thickness 0.01 m, respectively. Pressure maps on the $y = 0$ and $z = z_S$ planes are plotted in Fig. 10 at two different times considering the semi-infinite ground layer. The calculation is run over 1300 time iterations, which corresponds to a simulation time of 382 ms; the computational domain includes over 52 million points. This calculation is performed on a NEC SX-8 vector machine.

The spectra of the sound pressure level relative to the free field ΔL calculated numerically are compared with the spectra calculated analytically in Fig. 11 for receivers located 50 and 100 m away from the source in the $y = 0$ and $z = z_S$ planes. The top plots correspond to the Miki impedance model of a semi-infinite ground layer, and the bottom plots to the Miki impedance model of a rigidly backed layer of thickness 0.01 m. The numerical solution is in very good agreement with the analytical solution between approximately 20 and 600 Hz, with sound pressure level differences smaller than 1 dB. The sound pressure levels calculated numerically and analytically are then plotted in Fig. 12 with respect to the propagation distance x for six frequencies between 100 and 600 Hz; the receivers are still in the $y = 0$ and $z = z_S$ planes. Good agreement between the numerical and analytical solutions is found at all frequencies, with sound pressure level differences smaller than 1 dB.

V. Conclusions

In this paper, a general time-domain boundary condition (TDBC) has been proposed to include ground impedance models typically used in outdoor sound propagation applications in a linearized Euler equations solver. More specifically, the Miki model for a semi-infinite ground layer and for a rigidly backed layer of thickness d_L has been considered. This impedance model is simple, with one or two adjustable parameters, and meets the three necessary conditions for a model to be physically possible. To derive this TDBC, the impedance has been approximated by a sum of well-chosen template functions. The forms of these functions enable us to use the recursive convolution technique, which is very efficient from a numerical point of view. The impedance approximation can be performed in the frequency domain or in the time domain, and different methods have been described to identify the coefficients of the template functions. For the time-domain approximation, though, the response function $z(t)$ must be known analytically. The analytical expression of $z(t)$ for the Miki model of a semi-infinite ground layer has been derived in this paper.

Test cases in one- and three-dimensional geometries have been proposed to validate the TDBC. When only real poles λ_k are considered in the template functions, the numerical simulations become inaccurate when $\lambda_k \Delta t$ is large with respect to unity. For this reason, the method of optimization in the frequency domain, corresponding to a constrained nonlinear optimization, is preferred to the vector fitting algorithm to obtain the coefficients because the values of the poles cannot be easily bounded using vector fitting. The method of coefficient identification in the time domain also yields accurate numerical results, but has only been applied to the Miki model of a semi-infinite ground layer.

When the vector fitting algorithm has been applied to the Miki model of a rigidly backed layer of thickness 0.01 m, complex conjugated poles have been obtained. It has been seen that the calculations are not unconditionally stable in that case; unstable results occur when the imaginary part of the poles β_l is large. Finally, a configuration with a preferred propagation direction x has been considered. This is a more realistic geometry in the context of outdoor sound propagation. In these calculations, the frequency-domain optimization method has been used to obtain the coefficients of the TDBC. The numerical solution has been compared with an analytical solution in the frequency domain, and good agreement has been found over a large frequency band for propagation distances up to 100 m.

Based on these results, the method of optimization in the frequency domain can be recommended to identify the coefficients of the template functions, because it allows the values of the poles to be constrained and it can be applied to many impedance models. In the future, this coefficient identification method could be extended to consider a combination of real and complex conjugated poles. Real poles were sufficient to approximate the impedance models used in this study, but complex conjugated poles might be necessary to accurately approximate more complicated impedance models.

Appendix: Coefficients of the Time-Domain Impedance Boundary Conditions

The sets of coefficients obtained by the method of optimization in the frequency domain described in Sec. III.C are now given. The sets of coefficients OF v1 and OF v2, which correspond to the Miki impedance model of a semi-infinite ground layer, are described in Table A1, and the sets of coefficients OF v1L and OF v2L, which correspond to the Miki impedance model of a rigidly backed layer of thickness 0.01 m, are described in Table A2.

Table A1 Coefficients A_k and λ_k for the sets OF v1 and OF v2 relative to the Miki impedance model of a semi-infinite ground layer of effective flow resistivity 100 $\mathrm{kPa \cdot s \cdot m^{-2}}$

Coefficients	OF v1	OF v2
A_1	$1.414390450609 \times 10^6$	$1.574767007324 \times 10^6$
A_2	$1.001354674975 \times 10^6$	$1.619262374173 \times 10^6$
A_3	$-3.336020206713 \times 10^6$	$5.829632457408 \times 10^6$
A_4	$5.254549668250 \times 10^6$	$1.003332586572 \times 10^7$
A_5	$3.031704943714 \times 10^7$	——
λ_1	$5.233002301836 \times 10^1$	$6.860022583064 \times 10^1$
λ_2	$4.946064975401 \times 10^2$	$8.322958169623 \times 10^2$
λ_3	$1.702517657290 \times 10^3$	$9.381635897939 \times 10^3$
λ_4	$1.832727486745 \times 10^3$	$1.700000000000 \times 10^4$
λ_5	$3.400000000000 \times 10^4$	——

Table A2 Coefficients A_k and λ_k for the sets OF v1L and OF v2L relative to the Miki impedance model of a rigidly backed layer of thickness 0.01 and effective flow resistivity 100 $\mathrm{kPa \cdot s \cdot m^{-2}}$

Coefficients	OF v1L	OF v2L
A_1	$1.095250224109 \times 10^7$	$1.073949304469 \times 10^7$
A_2	$-4.880598235086 \times 10^5$	$-2.917377399830 \times 10^5$
A_3	$4.899396775177 \times 10^7$	$9.151005310626 \times 10^5$
A_4	$-7.739808262963 \times 10^7$	$-1.154537611236 \times 10^9$
A_5	$4.339456215283 \times 10^6$	$1.175832172629 \times 10^9$
A_6	$5.222037132729 \times 10^7$	$-9.893440512362 \times 10^6$
λ_1	$9.598920477807 \times 10^{-1}$	$5.211598094390 \times 10^{-1}$
λ_2	$8.685629982344 \times 10^1$	$1.479676658969 \times 10^2$
λ_3	$1.177170075809 \times 10^4$	$4.036203803055 \times 10^3$
λ_4	$1.381786001117 \times 10^4$	$1.386113814467 \times 10^4$
λ_5	$1.662539779506 \times 10^4$	$1.395977850813 \times 10^4$
λ_6	$3.212230274220 \times 10^4$	$1.407418372457 \times 10^4$

Acknowledgments

Support by Centre National de la Recherche Scientifique and Société Nationale des Chemins de Fer is gratefully acknowledged. Computing time was supplied by the Institut du Developpement et des Ressources en Informatique Scientifique, Centre National de la Recherche Scientifique.

References

[1] Salomons, E., Blumrich, R., and Heimann, D., "Eulerian Time-Domain Model for Sound Propagation Over a Finite-Impedance Ground Surface. Comparison with Frequency-Domain Models," *Acta Acustica United with Acustica*, Vol. 88, No. 4, 2002, pp. 483–492.

[2] Wilson, D., Collier, S., Ostashev, V., Aldridge, D., Symons, N., and Marlin, D., "Time-Domain Modeling of the Acoustic Impedance of Porous Surface," *Acta Acustica United with Acustica*, Vol. 92, No. 6, 2006, pp. 965–975.

[3] Zwikker, C., and Kosten, C., *Sound Absorbing Materials*, Elsevier, New York, 1949.
[4] Delany, M., and Bazley, E., "Acoustical Properties of Fibrous Absorbent Materials," *Applied Acoustics*, Vol. 3, No. 2, 1970, pp. 105–116. doi:10.1016/0003-682X(70)90031-9
[5] Attenborough, K., "On the Acoustic Slow Wave in Air-Filled Granular Media," *Journal of the Acoustical Society of America*, Vol. 81, No. 1, 1987, pp. 93–102. doi:10.1121/1.394938
[6] Bérengier, M., Stinson, M., Daigle, G., and Hamet, J., "Porous Road Pavement: Acoustical Characterization and Propagation Effects," *Journal of the Acoustical Society of America*, Vol. 101, No. 1, 1997, pp. 155–162. doi:10.1121/1.417998
[7] Rienstra, S., "Impedance Models in Time Domain Including the Extended Helmholtz Resonator Model," Twelfth AIAA/CEAS Aeroacoustics Conference, Cambridge, MA, AIAA Paper 2006-2686, 2006.
[8] Morse, P., and Feshbach, H., *Methods of Theoretical Physics*, Vol. 1, McGraw—Hill, New York, , 1953, pp. 370–373.
[9] Miki, Y., "Acoustical Properties of Porous Materials—Modifications of Delany-Bazley Models," *Journal of the Acoustical Society of Japan*, Vol. 11, No. 1, 1990, pp. 19–24.
[10] Berthelot, Y., "Surface Acoustic Impedance and Causality," *Journal of the Acoustical Society of America*, Vol. 109, No. 4, 2001, pp. 1736–1739. doi:10.1121/1.1352089
[11] Tam, C., and Auriault, L., "Time-Domain Impedance Boundary Conditions for Computational Aeroacoustics," *AIAA Journal*, Vol. 34, No. 5, 1996, pp. 917–923. doi:10.2514/3.13168
[12] Özyörük, Y., and Long, L., "A Time-Domain Implementation of Surface Acoustic Impedance Condition with and Without Flow," *Journal of Computational Acoustics*, Vol. 5, No. 3, 1997, pp. 277–296. doi:10.1142/S0218396X97000162
[13] Fung, K.-Y., and Ju, H., "Broadband Time-Domain Impedance Models," *AIAA Journal*, Vol. 39, No. 8, 2001, pp. 1449–1454. doi:10.2514/2.1495
[14] Reymen, Y., Baelmans, M., and Desmet, W., "Time-Domain Impedance Formulation Suited for Broadband Simulations," Thirteenth AIAA/CEAS Aeroacoustics Conference, Rome, Italy, AIAA Paper 2007-3519, 2007.
[15] Ostashev, V., Collier, S., Wilson, D., Aldridge, D., Symons, N., and Marlin, D., "Padé Approximation in Time-Domain Boundary Conditions of Porous Surfaces," *Journal of the Acoustical Society of America*, Vol. 122, No. 1, 2007, pp. 107–112. doi:10.1121/1.2743153
[16] Luebbers, R., and Hunsberger, F., "FDTD for Nth-Order Dispersive Media," *IEEE Transactions on Antennas and Propagation*, Vol. 40, No. 11, 1992, pp. 1297–1301. doi:10.1109/8.202707
[17] Chessell, C., "Propagation of Noise Along a Finite Impedance Boundary," *Journal of the Acoustical Society of America*, Vol. 62, No. 4, 1977, pp. 825–834. doi:10.1121/1.381603
[18] Rasmussen, K., "Sound Propagation Over Grass Covered Ground," *Journal of Sound and Vibration*, Vol. 78, No. 2, 1981, pp. 247–255. doi:10.1016/S0022-460X(81)80036-3
[19] Embleton, T., Piercy, J., and Daigle, G., "Effective Flow Resistivity of Ground Surfaces Determined by Acoustical Measurements," *Journal of the Acoustical Society of America*, Vol. 74, No. 4, 1983, pp. 1239–1244. doi:10.1121/1.390029
[20] Wilson, D., Ostashev, V., Collier, S., Symons, N., Aldridge, D., and Marlin, D., "Time-Domain Calculations of Sound Interactions with Outdoor Ground Surfaces," *Applied Acoustics*, Vol. 68, No. 2, 2007, pp. 173–200. doi:10.1016/j.apacoust.2005.10.004
[21] Kelley, D., and Luebbers, R., "Piecewise Linear Recursive Convolution for Dispersive Media Using FDTD," *IEEE Transactions on Antennas and Propagation*, Vol. 44, No. 6, 1996, pp. 792–797. doi:10.1109/8.509882
[22] Abramowitz, M., and Stegun, I., *Handbook of Mathematical Functions*, Dover, New York, 1965.
[23] Gustavsen, B., and Semlyen, A., "Rational Approximation of Frequency Domain Responses by Vector Fitting," *IEEE Transactions on Power Delivery*, Vol. 14, No. 3, 1999, pp. 1052–1301. doi:10.1109/61.772353
[24] Coleman, T., Branch, M. A., and Grace, A., Optimization Toolbox For Use with MATLAB User's Guide, Vers. 2, 1999.
[25] Bogey, C., and Bailly, C., "Large Eddy Simulations of Transitional Round Jets: Influence of the Reynolds Number on Flow Development and Energy Dissipation," *Physics of Fluids*, Vol. 18, No. 6, 2006, Paper 065101.
[26] Bogey, C., and Bailly, C., "A Family of Low Dispersive and Low Dissipative Explicit Schemes for Flow and Noise Computations," *Journal of Computational Physics*, Vol. 194, No. 1, 2004, pp. 194–214. doi:10.1016/j.jcp.2003.09.003
[27] Bogey, C., Cacqueray, N., and Bailly, C., "A Shock-Capturing Methodology Based on Adaptative Spatial Filtering for High-Order Non-Linear Computations," *Journal of Computational Physics*, Vol. 228, No. 5, 2009, pp. 1447–1465. doi:10.1016/j.jcp.2008.10.042
[28] Berland, J., Bogey, C., Marsden, O., and Bailly, C., "High Order, Low Dispersive and Low Dissipative Explicit Schemes for Multiple-Scale and Boundary Problems," *Journal of Computational Physics*, Vol. 224, No. 2, 2007, pp. 637–662. doi:10.1016/j.jcp.2006.10.017
[29] Bogey, C., and Bailly, C., "Three-Dimensional Non-Reflective Boundary Conditions for Acoustic Simulations: Far Field Formulation and Validation Test Cases," *Acta Acustica United with Acustica*, Vol. 88, No. 4, 2002, pp. 463–471.
[30] Tam, C., and Dong, Z., "Radiation and Outflow Boundary Conditions for Direct Computation of Acoustic and Flow Disturbances in a Nonuniform Mean Flow," *Journal of Computational Acoustics*, Vol. 4, No. 2, 1996, pp. 175–201. doi:10.1142/S0218396X96000040
[31] Rienstra, S., "1-D Reflection at an Impedance Wall," *Journal of Sound and Vibration*, Vol. 125, No. 1, 1988, pp. 43–51. doi:10.1016/0022-460X(88)90413-0
[32] Kelley, D., Destan, T., and Luebbers, R., "Debye Function Expansions of Complex Permittivity Using a Hybrid Particle Swarm-Least Squares Optimization Approach," *IEEE Transactions on Antennas and Propagation*, Vol. 55, No. 7, 2007, pp. 1999–2005. doi:10.1109/TAP.2007.900230
[33] Young, J., Kittichartphayak, A., Kwok, Y., and Sullivan, D., "On the Dispersion Errors Related to $(FD)^2TD$ Type Schemes," *IEEE Transactions on Microwave Theory and Techniques*, Vol. 43, No. 8, 1995, pp. 1902–1910. doi:10.1109/22.402280
[34] Beck, W., and Mirotznik, M., "Generalized Analysis of Stability and Numerical Dispersion in the Discrete-Convolution FDTD Method," *IEEE Transactions on Antennas and Propagation*, Vol. 48, No. 6, 2000, pp. 887–894. doi:10.1109/8.865220
[35] Zheng, S., and Zhuang, M., "Three-Dimensional Benchmark Problem for Broadband Time-Domain Impedance Boundary Conditions," *AIAA Journal*, Vol. 42, No. 2, 2004, pp. 405–407. doi:10.2514/1.9102
[36] Roseau, M., *Asymptotic Wave Theory*, North–Holland, Amsterdam, 1976, pp. 84–86.
[37] Blanc-Benon, P., Dallois, L., and Juvé, D., "Long Range Sound Propagation in a Turbulent Atmosphere Within the Parabolic Approximation," *Acta Acustica United with Acustica*, Vol. 87, No. 6, 2001, pp. 659–669.
[38] Cotté, B., and Blanc-Benon, P., "Estimates of the Relevant Turbulent Scales for Acoustic Propagation in an Upward Refracting Atmosphere," *Acta Acustica United with Acustica*, Vol. 93, No. 6, 2007, pp. 944–958.

D. Gaitonde
Associate Editor